Passive Sole Constraining Method to Stabilize 3D Passive Dynamic Walking

Naoto Mizoguchi and Sadayoshi Mikami
Graduate School of Systems Information Science
Future University Hakodate
Hakodate, Hokkaido, Japan
{g2118039@fun.ac.jp, s_mikami@fun.ac.jp}

Kazuyuki Hyodo
Department of Computer Science and Engineering
Fukuoka Institute of Technology
Fukuoka, Japan
hyodo@fit.ac.jp

Abstract— Inspired by the function of a toe and a lateral arch of a human foot, we propose a method to stabilize the biped walk by attaching unactuated toes and lateral arches. The toes and lateral arches work as adaptive braking of sagittal and lateral directions. They touch on the ground at the angle where the biped exceedingly inclines. After touching on the floor, the center of rotation changes at the landing positions. This change causes the reduction of the exceeding angular velocities toward sagittal and lateral directions. By setting appropriate heights of the toe and lateral arch during the swing phase, the walking robot is expected to be stabilized. To analyze the effects of the toe, we derived equations of motions and the state transition functions for a simplified 3D passive dynamic walker with toes. We clarified the potential stabilizing effect of the method from numerical simulations and preliminary experiments by a real-world biped with toes. Note that the proper setting of heights and the verification of the effect of lateral arches are on the way.

Keywords-biped; walk; stability; foot; toe; passive dynamic walk; equations of motion

I. INTRODUCTION

Walk stabilization of a biped robot is achieved mainly by controlling its posture and forces to apply on foot [1][2]. Floor reaction force control, which often referred to as ZMP based control, is a major method [1]. This method applies torques on ankles to move the ZMP inside the foot to maintain dynamical stability [2].

However, controlling ankles on a stance leg means driving both upper and lower bodies at once, which requires powerful torque on it [3]. This is energy inefficient and increases the difficulty to design appropriate actuators which demand both high torque and compactness.

Instead of 'driving' the supporting leg, we propose a method to control the angle, or the landing contact position, of the foot on the supporting leg [4][5]. This method is inspired by the function of a toe and a lateral arch of a human foot.

Fig.1 shows the movements of a landing foot during the stance phase in a typical human walk [6][7]. In a sagittal plane (right), the leg first rotates around the heel. Then, the toe touches on the ground, and the leg begins rotating around it, which is slightly ahead of the heel. As we describe later, the change of the center of rotation effects as braking the forward movement.

As we experience in daily life, when we walk down a slope, we put down our toe. By this, the change of the center of

rotation occurs earlier than the walk on flat ground, which effects as putting on the brake at an earlier time to prevent fall and body inclination. The same mechanism will be seen in the lateral plane (Fig.1 left). The height of the lateral arch is controlled by the ankle. The center of rotation in the lateral plane changes after the lateral arch touches on the ground. This change also effects as braking the side movement to keep stability over sideways.
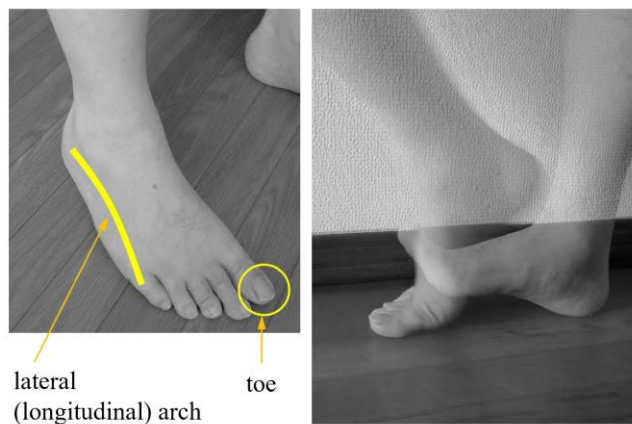

Figure 1. Change of rotation center by toe and lateral longitudinal arch of foot in human walk. Lateral rotation center change by lateral arch (left). Sagittal rotation center change by toe (right).

Sole constraining mechanism (toe) with height control. A servo motor changes the height of toe during swing phase.
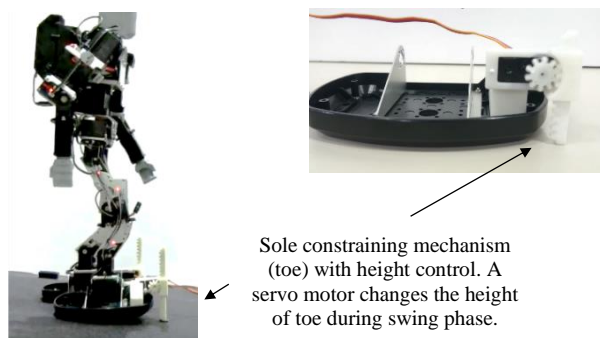
Figure 2. A small humanoid robot (KHR-3) attached with our sole constraining (toe) mechanism. The toe is driven by a servo motor which controls the height during swing phase.
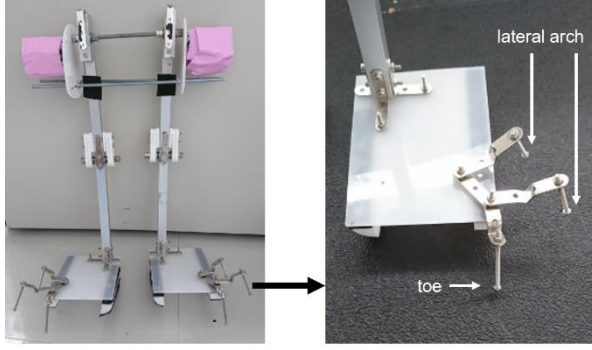
Figure 3. A 3D passive dynamic walker with knees and the toe and lateral arch mechanisms on foot. Experiments by this walker are described in section 5.

This stability control method by the change of the center of rotation is easily realized on the foot of a bipedal robot [4]. Fig. 2 shows our experimental sagittal mechanism of changing the height of a toe. In this design, a motor changes the height of the toe during swing phase. Since the toe is driven by a high gear ratio, it keeps the height during the stance phase. The adjustable toe realizes the change of the center of rotation at a different point without using powerful torque on foot. Fig. 3 is another realization of the toe and the lateral arch on a passive dynamic walker with knees. In this case, the heights of these constraints are chosen by hand to adapt to the slope. Usually, a passive dynamic 3D walker is unstable [8][9]. But the walker with these constraining devices exhibited high stability and able to continue walking for many steps.

One of the essential points to be clarified is the amount of height of the toe and the side arches to acquire stability. These should be set according to the condition of a walk, such as a road inclination angle. A mathematical model of the bipedal walking with the change of rotation center should be needed to derive the control rules. However, there has been no such model described.

This paper shows the dynamics model of a simplified 3D bipedal walk with the effect of the change of rotation center by the toe. We simulate the passive dynamic walk in this model. Since the stability of passive dynamic walk is known to be highly sensitive to its parameters such as initial conditions [10], it is an appropriate platform to discuss the effect of the toe. In our model, we will show that the effect of rotation around toe works to reduce the speed in the sagittal plane. We will also show that the model with the toe is more stable than the one without it under the environmental parameter changes. The reason is that the braking effect by toe rotation only occurs when the body inclines at a certain level (Fig. 4). In another word, the model automatically puts on the brake when it is too much inclining.
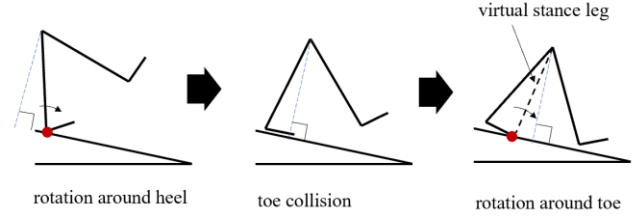

Figure 4. Change of the center of rotation before and after a toe collision (sagittal view). After the collision, a virtual link from hip to toe becomes a new stance leg.

This paper is organized as follows: First, we show the model of a simplified 3D biped with toe and lateral arch. Second, we derive the equations of motion and the equations of the transition of states by the stance-swing leg change and the toe grounding. Third, we show the results of the numerical simulations of our model and the model without a toe. The results of an actual 3D passive dynamic walk biped will be shown.

Note that the lateral arch effect and the toe height (angle) derivation according to the slope inclination are underway and are not included in this report.

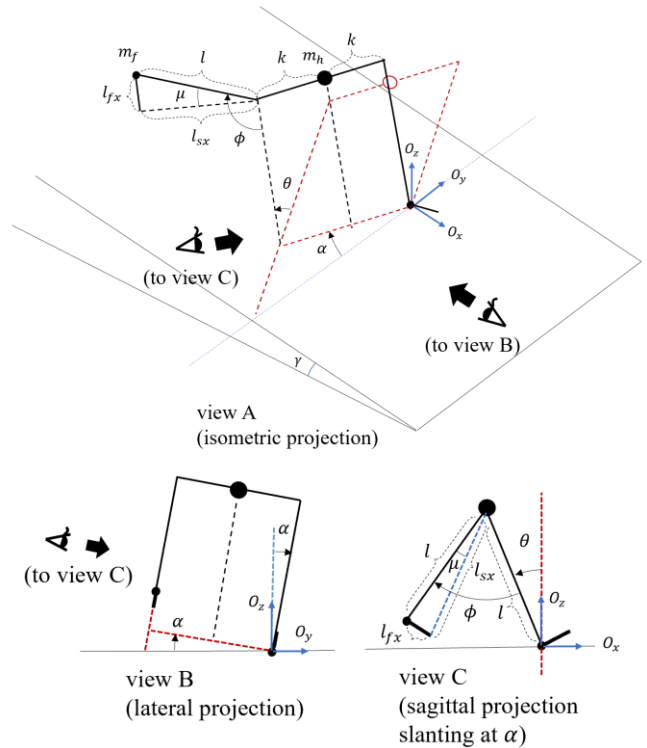## II.   3D PASSIVE DYNAMIC BIPED MODEL WITH TOES

Figure 5. A simplified point-mass 3D passive dynamic biped model with toes. The hip axle keeps in parallel to the Oy axis.

Fig. 5 shows the configuration of our model. It is based on Wisse and van der Linde's 'simplest passive walking model with lean-to-yaw coupling' [10]. This model assumes that the hip axle does not rotate around the yaw direction (around the 'Oz' axis in Fig. 5). The difference with the Wisse's model is that our model has a 'toe' fixed at the point-foot to the 'Ox' direction.

Fig. 5 (lower part) shows a projection of the model onto the sagittal plane slanting at α. The toe, which is indicated by a straight bold line, is affixed at the ankle at an angle μ which is specified by the leg length l, toe length l_{fx}, and the length l_{sx} from hip axle to the top of the toe. The stance leg rotates around the point leg (Fig. 4 left). Immediately after the toe touches the ground (i.e., the toe line lies on the floor), the stance leg rotates around the toe (Fig. 4 right).

The dynamics of the system is represented by a set of generalized coordinates $q = [\theta \ \phi \ \alpha]^{\mathrm{T}}$, which correspond to the stance leg hip joint angle, the swing leg hip joint angle, and the degree of sway in a lateral plane. The configuration parameters are $\{l, k, l_{fx}, l_{sx}, \gamma, m_h, m_f\}$, which correspond to the stance/swing leg length, half the width of the hip axle, the toe length, the length from hip axle to the toe, the slope inclination, the hip point mass, and the foot point mass (Fig. 5). Note that the foot point mass will be regarded as infinitely small during derivation of the equations of motion [10][11].

III. EQUATIONS OF MOTION AND TRANSITION RULES OF COLLISION

A. Equations of motion between collision

The equations of motion between collision of foot or toe is derived as the point-mass system [10].

First, the locations of the points of mass at stance foot, hip, and swing foot are written as

$r_1 = [0\ 0\ 0]^T$,
$r_2 = [-l\ sin\theta, -k\ cos\alpha + l\ sin\alpha\ cos\theta, k\ sin\alpha + l\ cos\alpha\ cos\theta]^T$,
$r_3 = \left[-l\ sin(\phi - \theta) + sin\theta, -2k\ cos\alpha - l\ (cos(\phi - \theta) - cos\theta)sin\alpha, 2k\ sin\alpha - l\left(cos(\phi - \theta)\right)cos\alpha\right]^T$. (1)

Second, The external force (gravitational force) applied to the stance foot, hip, and swing foot are represented as

$f_1 = [0\ 0\ 0]^T, f_2 = [m_h\ sin\gamma, 0, -m_h cos\gamma]^T$,
$f_3 = \left[m_f sin\gamma, 0, -m_f cos\gamma\right]^T$. (2)

From these, the generalized mass matrix M is given by

$M = m_f J_1^T + m_h J_2^T + m_f J_3^T$, (3)

where J_1, J_2, and J_3 are the Jacobians of r_1, r_2, and r_3 according to the generalized coordinates q. The generalized force Q^e is given by

$Q^e = J_1\ f_1 + J_2\ f_2 + J_3\ f_3$. (4)

Also the inertia force Q^v is calculated as

$Q^v = -m_f J_1^T J_1 \dot{q} - m_h J_2^T J_2 \dot{q} - m_f J_3^T J_3 \dot{q}$. (5)

Applying the *principle of virtual work* with these values leads to the equations of motion as

$M\ddot{q} = Q^e + Q^v$. (6)

The explicit form of the equations of motion is shown in the Appendix.

B. Transition rules of collision (1: toe collision)

In a passive walking model, the angles and the angular velocities change after the collision of the heel and the switching of swing and stance legs. In contrast to the point-foot model [11], our model with toe collides (1) at the toe of the stance leg and (2) at the heel of the swing leg. The transition rules of these collisions are derived as follows:

First, the collision of toe occurs in advance to the collision of the heel. Fig. 6 shows the rotation of the stance leg before and after the toe collision. Note that, in the following descriptions, we use superscript '-' and '+' for the state variables before and after the collision.

configuration parameters

during heel rotation

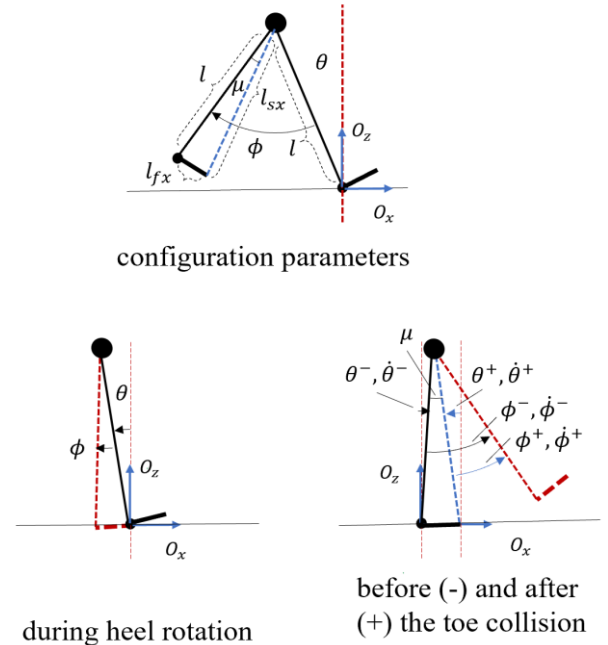before (-) and after (+) the toe collision

Figure 6. Change of angles and angular velocities before and after the toe collision.

As in the previous works [10][11], we assume that the ground contact at heel and toe are complete inelastic collision and the angular momentum around the contact points will be

reserved between collision [12]. From Fig. 6, the angular momentum around the toe before collision is calculated as

$$H_{toe}^- = m_h l_{sx} \, l \, \dot{\theta}^- \cos \mu, \tag{7}$$

where $\cos \mu = \dfrac{l^2 + l_{sx}^2 - l_{fx}^2}{2l \, l_{sx}}$. The angular momentum around the toe after collision becomes

$$H_{toe}^+ = m_h \, l_{sx}^2 \, \dot{\theta}^+. \tag{8}$$

$H_{toe}^- = H_{toe}^+$ leads to the new angular velocity after collision as

$$\dot{\theta}^+ = \dot{\theta}^- \frac{l^2 + l_{sx}^2 - l_{fx}^2}{2 \, l_{sx}^2}. \tag{9}$$

By the relative relationships of new and old stance/swing legs, the angle of the new stance and swing leg becomes

$$\begin{aligned} \theta^+ &= \theta^- + arccos\,\mu, \\ \phi^+ &= \phi^- + arccos\,\mu. \end{aligned} \tag{10}$$

Note that the angular velocities $\dot{\phi}$ and $\dot{\alpha}$ remain unchanged.

C. Transition rules of collision (2: swing-stance leg exchange)

Second, the collision of the swing leg heel occurs shortly after the change of the center of rotation of the stance leg (Fig. 5). Fig. 7 shows the relationship of the swing and stance legs before and after the collision of the heel of the new stance leg. A major difference with the normal walker is that the angle of the new swing leg is different from the former stance leg. This is because the former stance leg is rotating around its toe, and the new swing leg swings its heel (Fig. 7). From the figure, the angular momentum around the heel of the new stance leg (point C) before collision is

$$H_c^- = m_h \, ll_{sx} cos \, (\phi^- - \mu)\dot{\theta}^-. \tag{11}$$

The angular momentum of the new stance leg after collision is

$$H_c^+ = m_h \, l_{sx}^2 \, \dot{\theta}^-. \tag{12}$$

By the preservation of the momentum $H_c^- = H_c^+$, the new angular velocity after collision is given as

$$\dot{\theta}^+ = \dot{\theta}^- \frac{l}{l_{sx}} cos(\phi^- - \mu). \tag{13}$$

Also, the angular momentums around the hip axle before and after the collision are written as

$$H_B^- = 0 \text{ and } H_B^+ = m_f l(\dot{\phi}^+ + \dot{\theta}^+ - \dot{\theta}^+ cos\phi^+). \tag{14}$$

Assuming these to be equal, we derive the angular velocity of the new swing leg as

$$\dot{\phi}^+ = \dot{\theta}^+(1 - cos\phi^+). \tag{15}$$

We assume that the angular velocity of the sway motion α will be kept before and after the collision [12].

These equations are used in the numerical simulations described in the next chapter.
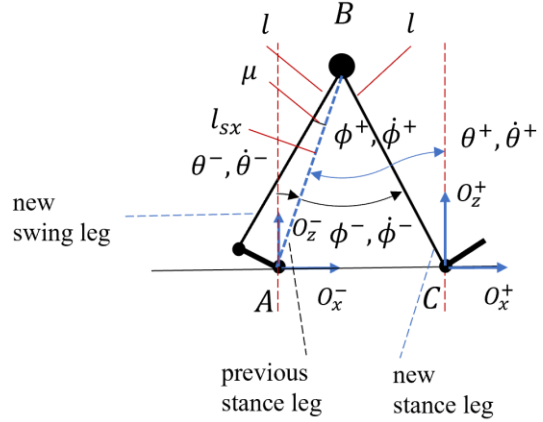

Figure 7. Change of angles and angular velocities before (-) and after (+) heel collision. Stance and swing leg exchange occurs. A new swing leg will be the link between the hip axle and the heel.

IV. NUMERICAL SIMULATIONS TO EVALUATE BRAKING AND STABILIZING EFFECT OF TOES

To evaluate the effect of braking and stability-enhancing effect of introducing toe, we conducted numerical simulations. Simulations of walking several slope inclinations were conducted. Each simulation runs for two steps (one walking cycle).

The configuration parameters of walker were set as follows:

$$\{l: 1 \, [m], k: 0.5 \, [m], l_{fx}: 0.2 \, [m], l_{sx}: 1.011 \, [m],$$
$$m_h: 1 \, [kg], m_f: (\text{infinitely small}), \text{gravitational force:}$$
$$9.8 \, [m/s]\}.$$

The initial conditions of movement were set as follows:

$$\{\theta: 1/6\pi \, [rad], \phi: 1/3\pi \, [rad], \alpha: 0 \, [rad],$$
$$\dot{\theta}: -1.79 \, [rad/s], \; \dot{\phi}: -1.79 \, [rad/s], \; \dot{\alpha}: 1.1 \, [rad/s]\}.$$

Note that the initial angular velocities are chosen so that the model without toe that is walking on a flat floor will resume the same states after heel collision. (Details of derivation of the values are omitted in this paper.)

Since the parameters are set for the flat ground walk ($\gamma = 0$), the simulations running at the conditions of $\gamma > 0$ will result in unstable walking. By observing the difference of angles and the angular velocities between the initial state and

the final state of the simulation, we will evaluate the stability of the model.

3D stick diagram of the model 'without toe'
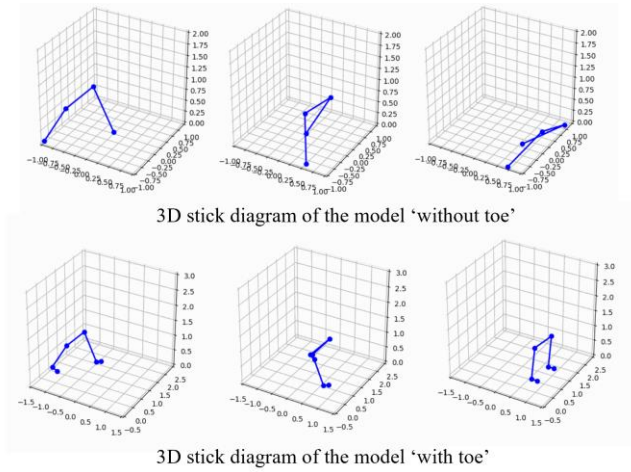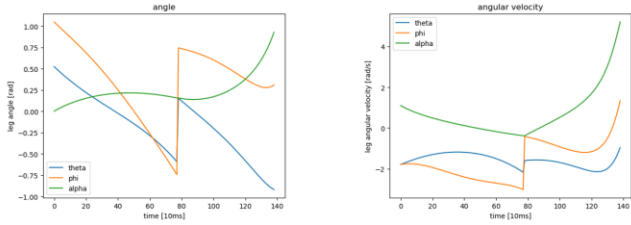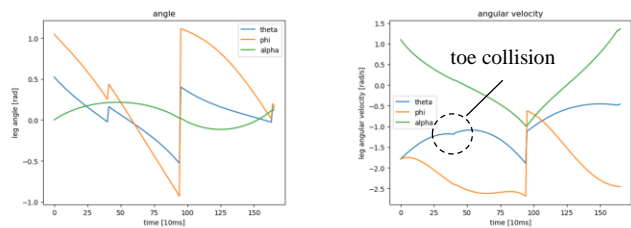
3D stick diagram of the model 'with toe'

Figure 8. 3D stick diagrams of the numerical simulation of the model. The upper and lower diagrams correspond to the results of the model without and with toe.

angle and angular velocities of the model 'without toe'

angle and angular velocities of the model 'with toe'

Figure 9. Angles and angular velocities of the numerical simulation of the model. The upper and lower diagrams correspond to the results of the model without and with toe.

Fig. 8 and 9 show the results of simulations with and without toe at the slop inclination $\gamma = 1.5$ [deg]. The upper half of the Fig.8 shows the 3D stick diagrams by the simulation of the model without toes, and the lower half shows the diagrams of the model with toes.

Both results exhibit the same stable walk during the first step. However, after the swing/stance leg change, the model without toe behaves unstable, whereas the model with toe keeps almost the same stable walk.

The left hand of Fig. 9 shows the change of angles. The right-hand shows the change of angular velocities. The upper part is for the model without toes, and the lower part shows the model with toes. In the graphs of the model with toes, the stance and swing legs angle had changed at around 300 [ms]. This step-change is caused by the change of the rotation center of the stance leg from heel to toe. As seen in the right figure, the angular velocities of stance and swing legs exhibit the reduction of absolute value at the time of the rotation center switching.

This reduction is the braking effect of the toe model. The effect occurs just after the toe touched on the ground (at 300 [ms] in this simulation). By this, we will expect the toe as a brake that automatically works when the stance leg inclines too much.

The angular velocities of the model without toe at the end of the simulation (mid of the second stride) showed a rapid increase, which means the model had fallen quickly. Instead, the model with toe achieves mostly the same profiles before and after the swing-stance leg exchange. It would be expected that the toe contributes to stabilizing the passive dynamic walk against the change of the environment.

V.   EXPERIMENTS BY REAL WORLD MODEL

To examine the effect of the change of rotation center by the toe and lateral arch, we conducted experiments by using a real-world passive dynamic walker. The walker is shown in Fig. 3. Unlike the simulation model, the walker has knees and is attached with pins that work as toes and lateral arches (Fig.3 right). The pink parts are the weights (0.45 [kg] each). The size of the walker is 300 [mm] height and 200 [mm] width. The foot shape consists of slightly rounding arch soles attached at both side edges.
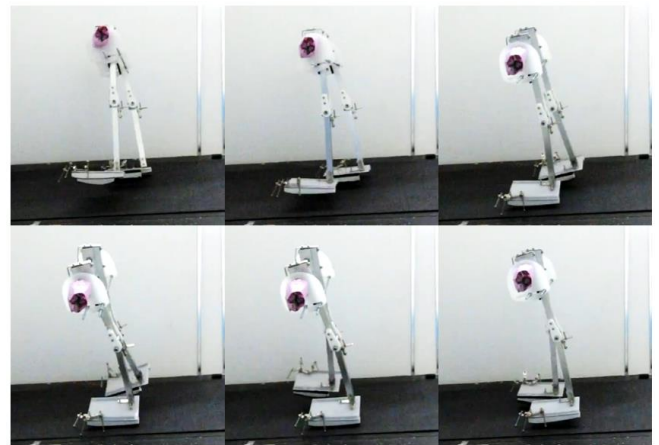

Figure 10. A sequence of pictures of the sagittal view of the real-world passive dynamic biped shown in Fig. 3. The order is from upper left to lower right.

The walking experiments were conducted on a treadmill inclining at 5.5 [deg]. The heights of pins are tuned by hand to achieve the walker's stability as high as possible. Therefore,

the experiments only show the potential of the introduction of toes and lateral arches.
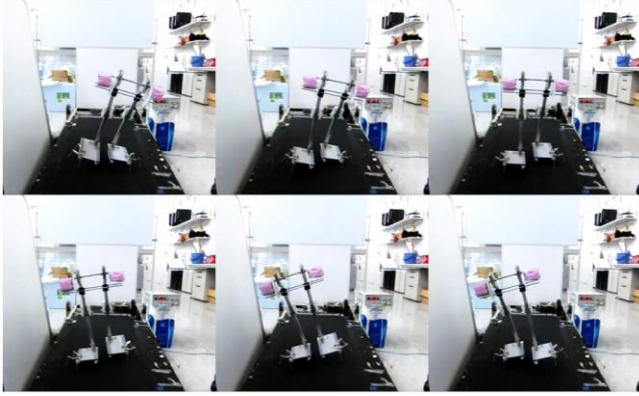

Figure 11. A sequence of pictures of the lateral view of the real-world passive dynamic biped shown in Fig. 3. The order is from upper left to lower right.

VI. Conclusions

We have proposed a stability enhancement method for a biped which uses unactuated 'toes' and 'lateral arches' on foot. Our idea was to use the braking effect by the change of rotation center caused by the toes and lateral arches. By appropriately pre-setting heights of toes and lateral arches, the braking effects take place during stance phase at the time when the stance leg begins to incline too much. We have shown the stabilization effect through the 3D simulations of a passive dynamic walker with toes. We have revealed the equations of motions and the state transition equations of the exchange of heel-toe rotations and swing-stance legs.

Our results showed the potential effectiveness of the toe. However, the derivation of appropriate heights of toes and lateral arches, and the dynamical and numerical analysis of the effect of lateral arches are still left for further researches.

As the passive constraint of the foot by toes and lateral arches does not use high motor torques and is easily attached on foot like shoes for a biped, we will continue to reveal control laws and more generic hardware designs.

References

[1] S. Kajita et al., "Biped walking pattern generation by using preview control of zero-moment point," in 2003 IEEE International Conference on Robotics and Automation (Cat. No. 03CH37422), 2003, vol. 2, pp. 1620–1626.

[2] E. R. Westervelt, J. W. Grizzle, C. Chevallereau, J. H. Choi, and B. Morris, Feedback control of dynamic bipedal robot locomotion. CRC press, 2018.

[3] S. Kajita and B. Espiau, "Legged robots," Springer handbook of robotics, pp. 361–389, 2008.

[4] K. Hyodo, Y. Iwaguchi, Y. Takamura, and S. Mikami, "Stability Effect for Passive Dynamic Walker by Stance Leg Heel Angle Constraint Using Foot Shape," in The First International Symposium on Swarm Behavior and Bio-Inspired Robotics (SWARM 2015), Kyoto, Japan, 2015, pp. 473–477.

[5] K. Hyodo, T. Oshimura, S. Mikami, and S. Suzuki, "Stabilizing Passive Dynamic Walk Under Wide Range of Environments by Constraint Mechanism Fitted to Sole of Foot," Journal of Robotics and Mechatronics, vol. 21, no. 3, pp. 403–411, 2009.

[6] J. Rose and J. G. Gamble, Human Walking. Lippincott Williams & Wilkins, 2006.

[7] D. A. Winter, "Human balance and posture control during standing and walking," Gait & posture, vol. 3, no. 4, pp. 193–214, 1995.

[8] S. H. Collins, M. Wisse, and A. Ruina, "A three-dimensional passive-dynamic walking robot with two legs and knees," The International Journal of Robotics Research, vol. 20, no. 7, pp. 607–615, 2001.

[9] S. H. Collins and A. Ruina, "A bipedal walking robot with efficient and human-like gait," in Proceedings of the 2005 IEEE international conference on robotics and automation, 2005, pp. 1983–1988.

[10] M. Wisse and R. Q. Van der Linde, Delft pneumatic bipeds, vol. 34. Springer Science & Business Media, 2007.

[11] M. Garcia, A. Chatterjee, A. Ruina, and M. Coleman, "The simplest walking model: stability, complexity, and scaling," Journal of biomechanical engineering, vol. 120, no. 2, pp. 281–288, 1998.

[12] H. Herr and M. Popovic, "Angular momentum in human walking," Journal of experimental biology, vol. 211, no. 4, pp. 467–481, 2008.

[13] A. Yamamoto, S. Fujimoto, and T. Kinugasa, "3D Quasi-passive Walking of Biped Robot with Flat Feet-Gait Comparison between Passive Walking and Quasi-passive Walking," International Journal of Advanced Materials and Production, vol. 1, no. 1, pp. 14–20, 2016.

Appendix

The explicit forms of the equations of motions are shown below. Note that the font size is intentionally reduced due to the limitation of page length.

$$\frac{d^2\theta}{dt^2} = \frac{0.2k\left(5.0kl\cos(\theta(t))\left(\frac{d}{dt}\theta(t)\right)^2 - 49.0k\cos(\gamma)\cos(\alpha(t)) + 5.0l^2\sin(2.0\theta(t))\frac{d}{dt}\alpha(t)\frac{d}{dt}\theta(t) + 49.0l\sin(\alpha(t))\cos(\gamma)\cos(\theta(t))\right)\sin(\theta(t))}{-0.1(k^2 + l^2\cos^2(\theta(t)))\left(5.0l\sin(2.0\theta(t))\left(\frac{d}{dt}\alpha(t)\right)^2 + 98.0\sin(\gamma)\cos(\theta(t)) - 98.0\sin(\theta(t))\cos(\gamma)\cos(\alpha(t))\right)}{(l(k^2 + l^2)\cos(\theta(t)))}$$

$$\frac{d^2\alpha}{dt^2} = \frac{kl\cos^2(\theta(t))\left(\frac{d}{dt}\alpha(t)\right)^2 - kl\left(\frac{d}{dt}\alpha(t)\right)^2 + kl\left(\frac{d}{dt}\theta(t)\right)^2 - 9.8k\sin(\gamma)\sin(\theta(t))}{-9.8k\cos(\gamma)\cos(\alpha(t))\cos(\theta(t)) + 2.0l^2\sin(\theta(t))\frac{d}{dt}\alpha(t)\frac{d}{dt}\theta(t) + 9.8l\sin(\alpha(t))\cos(\gamma)}{(k^2 + l^2)\cos(\theta(t))}$$

$$\frac{d^2\phi}{dt^2} = \frac{0.1\left(\begin{array}{c} -2.0k\left((\cos(\phi(t) - 1.0)\sin(\theta(t))) + 2.0\sin(\phi(t) - \theta(t))\right) \\ +(k^2 + l^2)\left(\begin{array}{c} 5.0kl\cos(\theta(t))\left(\frac{d}{dt}\theta(t)\right)^2 - 49.0k\cos(\gamma)\cos(\alpha(t)) \\ +5.0l^2\sin(2.0\theta(t))\frac{d}{dt}\alpha(t)\frac{d}{dt}\theta(t) + 49.0l\sin(\alpha(t))\cos(\gamma)\cos(\theta(t)) \end{array}\right) \\ +(k^2 + l^2)\left(\begin{array}{c} 5.0l\sin(\phi(t) - 2.0\theta(t))\left(\frac{d}{dt}\alpha(t)\right)^2 - 5.0l\sin(2.0\phi(t) - 2.0\theta(t))\left(\frac{d}{dt}\phi(t)\right)^2 + 5.0l\sin(\phi(t))\left(\frac{d}{dt}\alpha(t)\right)^2 \\ +10.0l\sin(\phi(t))\left(\frac{d}{dt}\theta(t)\right)^2 - 98.0\sin(\gamma)\cos(\phi(t) - \theta(t)) - 98.0\sin(\phi(t) - \theta(t))\cos(\gamma)\cos(\alpha(t)) \end{array}\right)\cos^2(\theta(t)) \\ + \left(2.0k^2\sin(\phi(t) - \theta(t))\sin(\theta(t)) + (k^2 + l^2\cos^2(\theta(t)))(\cos(\phi(t)) - 1.0)\right) \\ \left(5.0l\sin(2.0\theta(t))\left(\frac{d}{dt}\alpha(t)\right)^2 + 98.0\cos(\gamma)\cos(\theta(t)) - 98.0\sin(\theta(t))\cos(\gamma)\cos(\alpha(t))\right) \end{array}\right)}{l(k^2 + l^2)\cos^2(\theta(t))}$$